Nanoparticle Synthesis

International Edition: DOI: 10.1002/anie.201506415
German Edition: DOI: 10.1002/ange.201506415

Polymer Cages as Universal Tools for the Precise Bottom-Up Synthesis of Metal Nanoparticles

*Ziyin Fan, Xuelian Chen, Melissa Köhn Serrano, Holger Schmalz, Sabine Rosenfeldt, Stephan Förster, Seema Agarwal, and Andreas Greiner**

Abstract: *A template synthesis allows the preparation of monodisperse nanoparticles with high reproducibility and independent from self-assembly requirements. Tailor-made polymer cages were used for the preparation of nanoparticles, which were made of cross-linked macromolecules with pendant thiol groups. Gold nanoparticles (AuNPs) were prepared in the polymer cages in situ, by using different amounts of cages versus gold. The polymer cages exhibited a certain capacity, below which the AuNPs could be grown with excellent control over the size and shape. Control experiments with a linear diblock copolymer showed a continuous increase in the AuNP size as the gold feed increased. This completely different behavior regarding the AuNP size evolution was attributed to the flexibility of the polymer chain depending on cross-linking. Moreover, the polymer cages were suitable for the encapsulation of AgNPs, PdNPs, and PtNPs by the in situ method.*

Template-mediated synthesis enables the preparation of monodisperse nanomaterials with predetermined sizes and shapes. The resulting nanocomposites are of interest in the fields of sensorics,[1,2] nanoelectronics,[3,4] biotechnology,[5] and heterogeneous catalysis.[6,7] Different types of templates, such as hollow nanocapsules[8–10] and nanocages,[11,12] have been investigated to improve the compatibility and stability of nanocomposites, particularly for the synthesis of spherical metal nanoparticles (NPs). Polymer capsules have been prepared as templates by the layer-by-layer (LbL) deposition of polyelectrolytes onto sacrificial templates[13,14] or by post-cross-linking of grafted polymer brushes on the NP surfaces.[15,16] The generated polymer networks usually exhibit dense polymer layers with good stability.[17,18] The quantitative functionalization of these networks usually depends on the nature of the polymers.[19] Cages with a well-defined structure, such as organic molecular cages or especially dendritic cages, are promising candidates for the precise stoichiometric functionalization of the templates, as they exhibit a monolayer with distinct anchor groups.[20] For example, dumbbell-like assemblies of AuNPs were prepared by the homocoupling of monofunctionalized AuNPs as artificial molecules.[21] However, the size of the NPs in such cages was limited to 1–2 nm, which demonstrates that increasing the size of the encapsulated NPs remains a challenge.

The advantage of templates with controlled functionality is the ability to precisely functionalize the encapsulated metal NPs by simple bottom-up approaches, which enables the further manipulation of NP aggregates. For stoichiometric control over the functionality of the NPs, our group developed an efficient "grafting-around" approach, which involves a one-step synthesis that generates monofunctionalized NPs wrapped with a cross-linked polymer chain.[22] The monofunctionalized NPs were further utilized as artificial molecules, which offers the potential for new versatile applications of the "grafting-around" concept.[23,24] Recently, we have shown that polymer cages prepared by "grafting-around" can be used for the size-selective separation of colloidal AuNPs.[25]

Based on the polymer cage concept, we developed a highly versatile tool for the precise bottom-up synthesis of metal NPs, which we report here with its possibilities and limitations. This concept was extended to AgNP, PdNP, and PtNPs to demonstrate the versatility of the cages. The clear outcome of this study is that polymer cages are superior templates with respect to size control for metal NPs than conventional diblock copolymers such as polystyrene-*block*-poly(4-vinylpyridine) (PS-*b*-PVP).

The concept for the precision bottom-up synthes1s of metal NPs by the use of polymer cages as templates is depicted schematically in Figure 1. First, AuNPs **1** coated with 4-vinylbenzenethiol were prepared. The following step is the "grafting-around" approach, where the polymerization of the vinyl-carrying ligands on AuNPs **1** was initiated by 4,4′-azobis(4-cyanovaleric acid), which led to a polymer network with a single carboxylate functionality originating from the initiator (AuNPs **2**). Subsequently, the carboxylate group on AuNPs **2** was reacted with 4-vinylaniline, which resulted in vinyl-functionalized AuNPs **3**, which were copolymerized with methyl methacrylate (MMA; AuNP-*co*-PMMA). The

[*] Z. Fan, M. Köhn Serrano, Dr. H. Schmalz, Prof. Dr. S. Agarwal, Prof. Dr. A. Greiner
Chair of Macromolecular Chemistry II and Bayreuth Centre for Colloids and Interfaces
University of Bayreuth
Universitätsstrasse 30, 95440 Bayreuth (Germany)
E-mail: greiner@uni-bayreuth.de
Homepage: http://www.mcii.uni-bayreuth.de/en/ag-greiner/index.html
Dr. X. Chen, Dr. S. Rosenfeldt, Prof. Dr. S. Förster
Chair of Physical Chemistry I
University of Bayreuth (Germany)

Supporting information for this article (including experimental details) is available on the WWW under http://dx.doi.org/10.1002/anie.201506415.

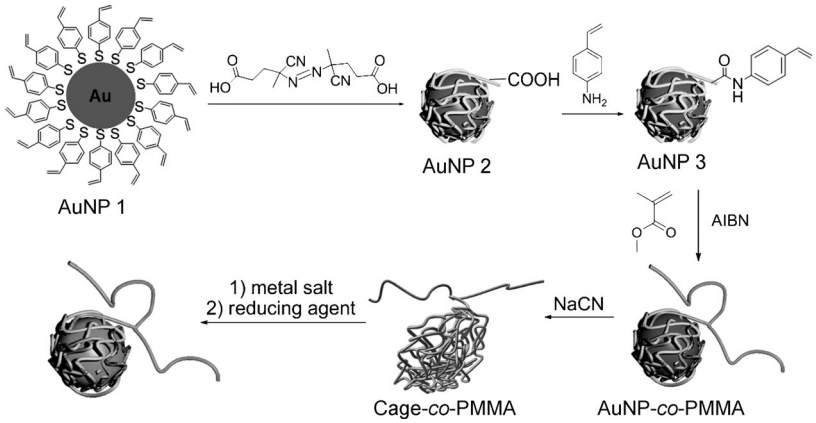

Figure 1. Synthesis of the polymer cage by the "grafting-around" approach and subsequent encapsulation of precious-metal nanoparticles by the in situ method. AIBN = azobis(isobutyronitrile).

size [(4.5 ± 2.2) nm] of the AuNPs remained the same during the whole procedure (characterization data are shown in the Supporting Information, Figures S1 and S2). The polymer cage (Cage-*co*-PMMA), namely, the cross-linked macromolecule shell around the AuNP surface, was prepared by etching the AuNPs using sodium cyanide (NaCN; characterizations are given in Figures S3 and S4). The polymer cages were cross-linked by chain transfer or entanglement during polymerization and by the formation of disulfide bonds from thiolates during oxidative etching. As the vinyl-polymerizable ligands were distributed on the AuNP surface, the resulting macromolecules were wrapped around the AuNPs and, thus, were more flexible than hollow capsules with much thicker shells.[25]

The size of the AuNPs is tunable through alteration of the molar ratio between the Au and ligand.[26] Thus, we anticipated a deviation from the known size evolution for encapsulated AuNPs prepared using Cage-*co*-PMMA templates. To test this, the Cage-*co*-PMMA templates were refilled with different Au feeds by in situ synthesis. For control experiments, we chose the linear diblock copolymer PS-*b*-PVP, whose pyridine moieties served as ligands for the AuNPs. We aimed to investigate how the flexibility/morphology of the polymer chain (here the polymer cage was cross-linked, whereas PS-*b*-PVP is non-cross-linked) influences the stability/size evolution of the encapsulated NPs (characterizations of PS-*b*-PVP are given in Figures S5–S8). The Au concentration was maintained at 1 mM, whereas the polymer concentrations were adjusted to the desired Au/polymer molar ratios. Upon addition of the reducing agent, the Au^{III} ions were reduced to Au^0, whereas the disulfide bonds were cleaved to thiolates. Therefore, the disulfide cross-linking did not play a role in the in situ synthesis. To focus on a comparison of the trend of the AuNP size evolution in different polymer matrices, the size evolution of AuNPs in the Cage-*co*-PMMA was controlled by using the equivalent amount of Au in the feed as was originally used in the AuNP-*co*-PMMA synthesis (equiv(Au)). In the control experiments, the relationship between the AuNP size and the molar ratio between Au in the feed and PS-*b*-PVP (Au/PS-*b*-PVP) was investigated. The Au/ligand molar ratios are given in Table S1.

Figure 2a presents transmission electron microscopy (TEM) images and the representative small-angle X-ray scattering (SAXS) data of AuNPs synthesized in Cage-*co*-PMMA. As the equiv(Au) was increased from 0.25 equiv to 0.75 equiv, only spherical AuNPs with a diameter of (4 ± 1.1) nm were observed by TEM analysis (the histograms are given in Figure S9). Very large particles are formed when equiv(Au) was increased from 1.00 equiv to 1.67 equiv and SAXS was performed to estimate the particle size (radius of gyration R_g) as well as obtain an indication of the nature of scattering inhomogeneities inside the sample. The investigated samples include nonsymmetrical particles or fractals. The data could not be described by the model of spheres. Nevertheless, the scattering intensity can be described by the Guinier–Porod approach [Eqs. (1) and (2)].

$$I(q) \propto \frac{1}{q^s}\exp\left(\frac{R_g^2}{3-s}\right) \quad (1)$$

$$I(q) \propto \frac{1}{q^d} \quad (2)$$

The size (R_g) and dimensionality (s; $s = 0$ for spheres, $s = 1$ for rods, and $s = 2$ for lamellae) of the object is included in the Guinier term. The Porod term is sensitive to inhomogeneities. For example, an exponent of $d = 4$ may arise from surface fractals or from the scattering of 3D objects such as spheres with a smooth surface, whereas an exponent of $d = 3$ can point to a collapsed polymer chain or to spheres with a rough surface. The radius of gyration of the AuNPs increased from 2.8 nm to 11.8 nm as equiv(Au) was increased from 0.25 to 1.67. At the same time, the Porod exponent changed from $d =$ 3.1 to $d = 3.8$. An equiv(Au) < 0.75 led to the low q range exhibiting an upturn in intensity. This trend vanishes as the Cage-*co*-PMMA content decreases. Such a progress can be caused by a non-negligible amount of objects with $R_g = 47$ nm (corresponding to a sphere with a radius of 60 nm). This phase was described as the "undersaturated" phase, where the AuNP size increased slightly (from $R_g = 2.8$ nm to 4.5 nm). Here, the presence of excessive Cage-*co*-PMMA allows control over the size and size distribution of the AuNPs. Upon a further increase of the equiv(Au) from 1.00 equiv to 1.67 equiv, the AuNPs immediately formed large aggregates (11.8 nm), which was described as the "oversaturated" phase. The characterization (TEM and SAXS) of each sample is given in Figure S9. We attributed this sharp transition from a controlled growth to a sudden agglomeration as a result of the cage deficiency, which clearly demonstrated the role of Cage-*co*-PMMA as a stabilizing template for the AuNPs. The UV/Vis spectra of AuNPs in Cage-*co*-PMMA are shown in Figure S10, left.

The behavior of PS-*b*-PVP in terms of the AuNP size evolution was significantly different from that when cages

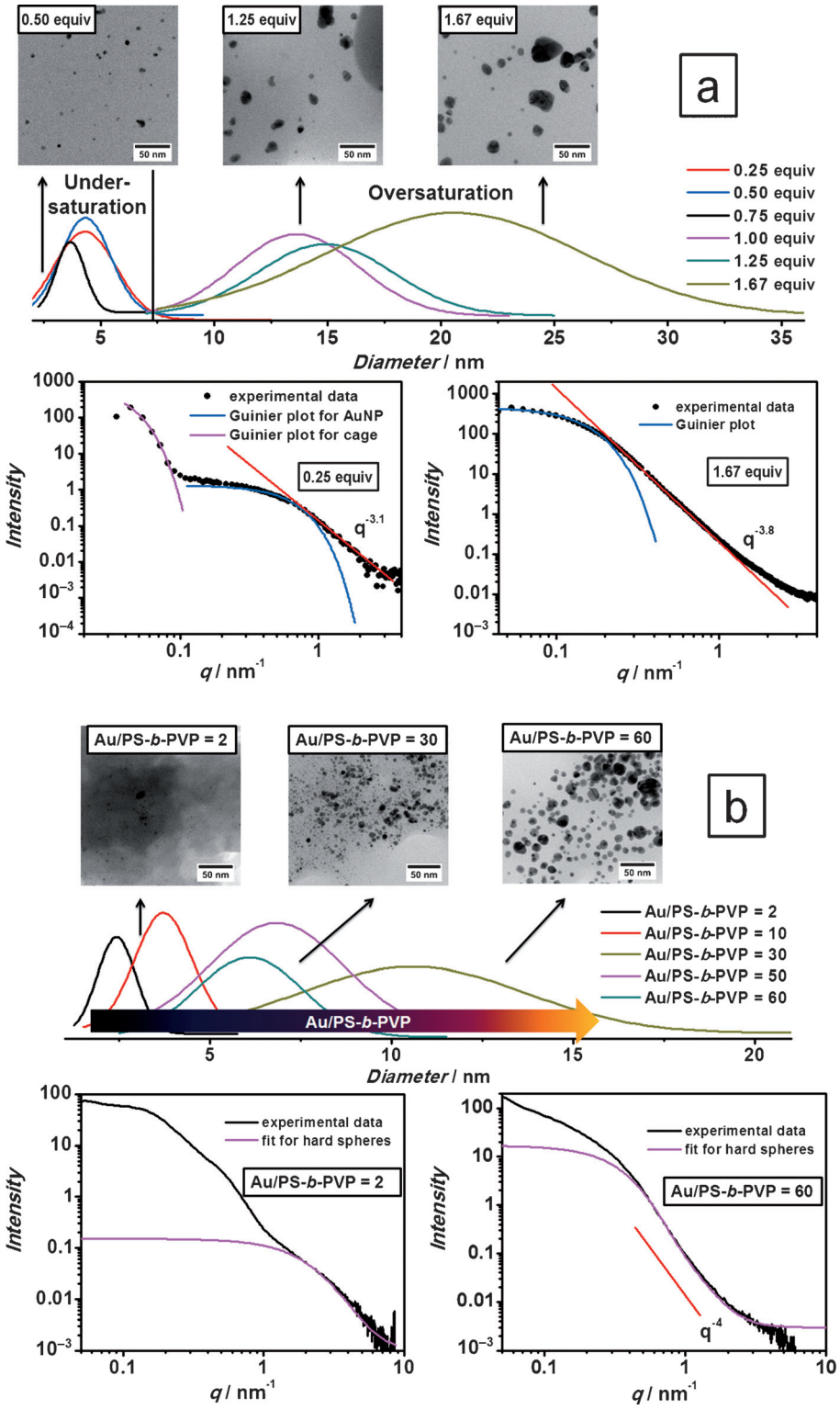

Figure 2. Comparison of the size evolution of AuNPs in a) Cage-*co*-PMMA and b) PS-*b*-PVP. Top: Gauss fit of the histograms of the AuNP size and size distribution with representative TEM images of various Au contents (equiv is denoted as the equiv(Au) for Cage-*co*-PMMA; Au/PS-*b*-PVP for the molar ratio between Au and PS-*b*-PVP). Representative SAXS data are shown below. Red trace: slope $= q^{-3.1}$ [(a), 0.25 equiv], $q^{-3.8}$ [(a), 1.67 equiv], q^{-4} (b); pink trace in (b): scattering of spheres having Schultz–Zimm distribution.

were used as templates (Figure 2b). A continuous growth of the AuNPs from (2.6 ± 0.7) nm to (11.6 ± 3.4) nm was observed in TEM micrographs on increasing the Au/PS-*b*-PVP ratios. At higher Au/PS-*b*-PVP ratios, the fraction of small AuNPs decreased, whereas the amount of large AuNPs increased constantly. The increase in the AuNP size with increasing Au/PS-*b*-PVP ratio was also confirmed by the SAXS data, which yielded AuNP diameters ranging from 2.4 nm to 14 nm (Figure 3, bottom). It is worth noting that for small q values the size is dominated by the PS-*b*-PVP and aggregates as evidenced by a sudden increase in $I(q)$, thus the SAXS curves are fitted at higher q values with spherical shape instead of Guinier approximation at low q range. TEM and SAXS analyses of each sample are given in Figure S11. Eventually, the AuNPs aggregated completely and precipitated (data not shown; the UV/Vis spectra are shown in Figure S10, right.)

The experimental observations are explained by the differences between the cage structure of Cage-*co*-PMMA and the linear chain structure of PS-*b*-PVP (Figure 4). At a high concentration of the cage in the "undersaturated" phase, the AuNPs were separately wrapped within a single Cage-*co*-PMMA. The diameter of the AuNPs, therefore, remained constant at approximately 5 nm with a narrow distribution (standard deviation less than 30%). When the Au content exceeded the capacity maximum of the cage, the cross-linked cages were not able to delocalize and, thus, not able to distribute the ligands homogeneously around the AuNP surface because of the entropic effect. This insufficient distribution of ligands created large defect sites on the surface of the AuNPs that significantly decreased the stability of the AuNPs. As a consequence, the AuNPs aggregated at these bare areas to reduce the surface energy and formed irregular-shaped agglomerates in the "oversaturated"

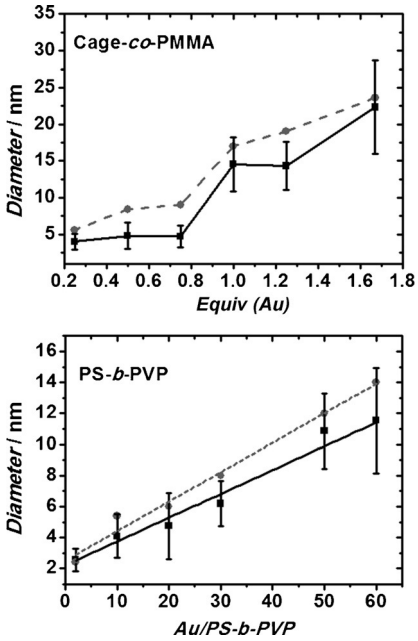

Figure 3. Plot of the AuNP size change derived by TEM (black solid trace) and SAXS (gray dotted trace) data as a function of Au equivalents (equiv(Au)) in the feed for Cage-*co*-PMMA (top) and the Au/PS-*b*-PVP molar ratio for PS-*b*-PVP templates (bottom).

phase.[26] In contrast, the PVP blocks of PS-*b*-PVP were rearranged on the AuNP surface until they were distributed homogeneously. Therefore, the AuNPs were stabilized over a large range of Au/PS-*b*-PVP ratios. However, the size distribution of the AuNPs was always broad due to Ostwald ripening or coalescence during the later growth state.[27]

The versatility of the "grafting-around" approach for precisely synthesized AuNPs templated by polymer cages was also applied to other metals. Sulfur ligands in the polymer cages are well known to be stabilizers for various precious-metal NPs. Here, the syntheses of AgNPs, PdNPs, and PtNPs were investigated using Cage-*co*-PMMA as a template. All reactions were carried out in the "undersaturated" regime (0.8 equiv of the metal salt in the feed).

According to the TEM results (Figure 5), the AgNPs were spherical, with a mean diameter of (6.2 ± 2.4) nm. SAXS analysis indicated a larger average diameter $(10.2 \pm 2.2$ nm). Aggregation was indicated by the up-turn in the low q region.[28] Rod-shaped PdNPs and PtNPs were observed (additional TEM images, histograms, and UV/Vis spectra are given in Figures S12 and S13). Similar structures were also observed for PdNPs synthesized by the in situ method in the presence of polymer ligands.[29] The formation of nanorods was attributed to the aggregation of primary spherical NPs. Often, the nanoparticles were so labile that they formed large aggregates with a wormlike substructure. However, in our case, the formation of large aggregates was suppressed. The dispersions were stable, even after three months under ambient conditions. Rodlike structures were indicated by the scaling of $q^{-1.2}$. This low shape control of the polymer cage is speculatively explained by a certain flexibility of Cage-*co*-PMMA, which enabled the anisotropic growth of nanoparticles within the cage.

In summary, monofunctionalized polymer cages with cross-linked polymer chains were used as efficient templates for the size-controlled bottom-up synthesis of metal NPs. A series of in situ syntheses of AuNPs in Cage-*co*-PMMA using feeds with various Au concentrations demonstrated the relationship between the cage structure and the size evolution of the encapsulated NPs. The AuNPs underwent a sharp transition from a controlled and uniform size and shape to agglomeration when the maximum loading capacity of the cages was exceeded. Control experiments with a linear diblock copolymer (PS-*b*-PVP) under comparable conditions did not provide any size control over the AuNPs. A plausible explanation for the inefficiency of PS-*b*-PVP is its chain flexibility. The size evolution of the AuNPs depends, to a large extent, on the distribution of the polymer chains on the surface of the AuNPs and on how the polymer chains adapt during nanoparticle growth, which is strongly linked to the chain flexibility. In turn, this unprecedented cage cross-linking was indirectly

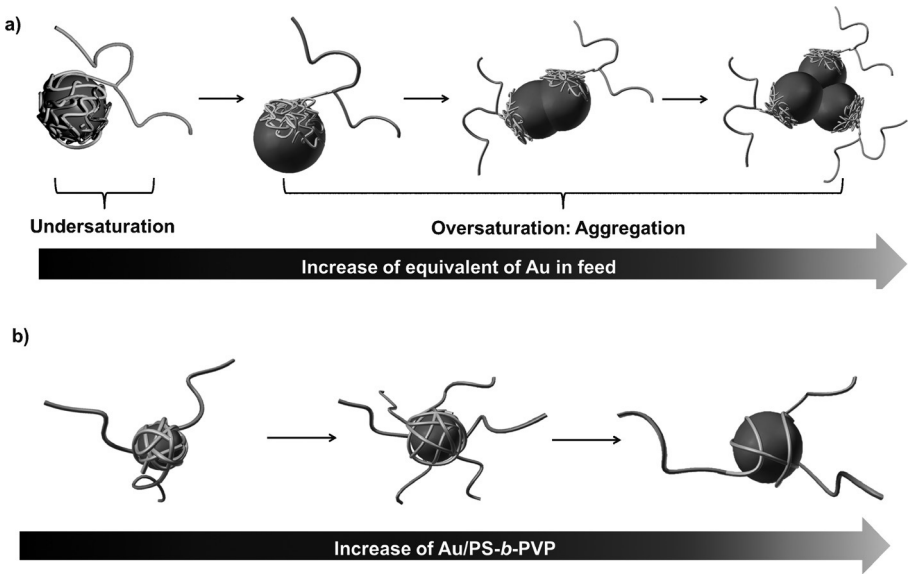

Figure 4. Size evolution of AuNPs in different templates. a) Isolated AuNPs with controlled size in the "undersaturated" phase were completely wrapped within single Cage-*co*-PMMA templates. As soon as the Au content exceeded the capacity of the Cage-*co*-PMMA, only some of the AuNPs could be stabilized by the cages because of their cross-linked structure ("oversaturated" phase). Consequently, the AuNPs aggregated. b) In the case of PS-*b*-PVP templates, the surface coverage decreased as the Au/PS-*b*-PVP molar ratio increased. The polymer chains were always homogeneously distributed around the AuNP surface, thereby resulting in a continuous growth of spherical AuNPs.

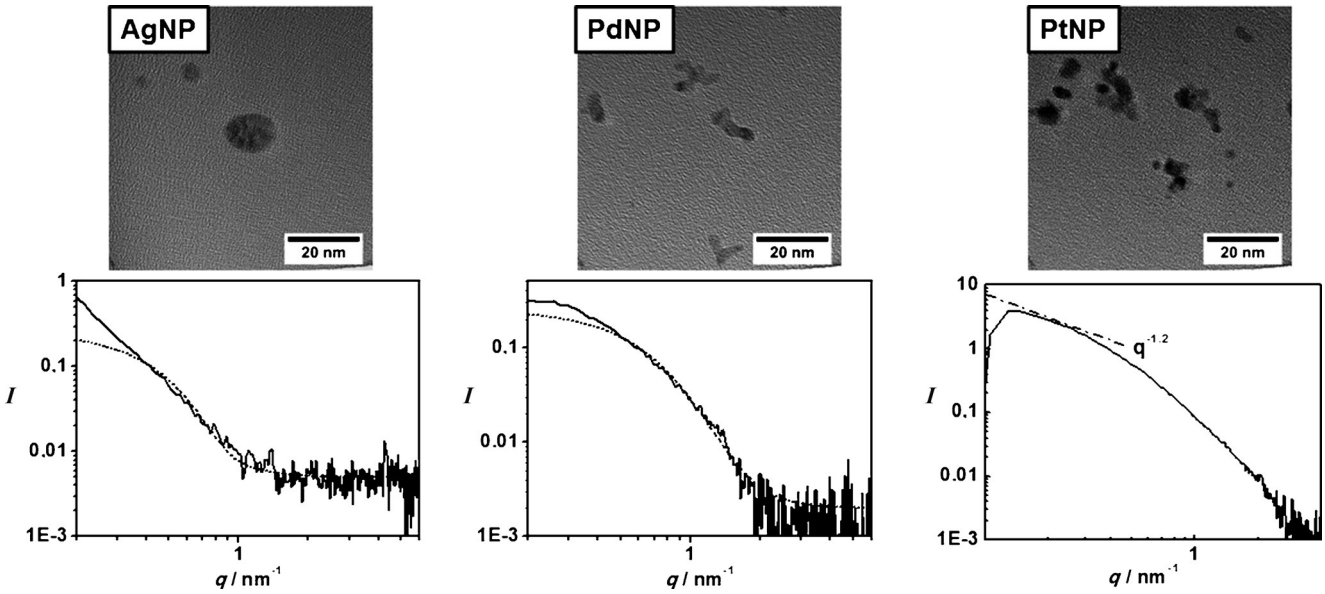

Figure 5. Representative TEM micrographs (top) and SAXS data (bottom; black trace: experimental data; gray dotted trace for AgNPs and PdNPs: fit for hard spheres, Schultz–Zimm distribution; black dotted trace for PtNP: scaling of $q^{-1.2}$) of metal NPs in Cage-*co*-PMMA prepared by the in situ method.

confirmed by this size evolution study, which revealed the polymerization mechanism on an NP surface in the sub-5 nm range. In upcoming studies we aim to prepare the polymer cages with controllable sizes, thus increasing the scope of size control of general NP syntheses. For example, through selecting the proper cage size and amount, AuNPs with sizes of 10 nm and 50 nm can be produced in one pot with desired populations. The grafted sulfur moieties make Cage-*co*-PMMA a universal template for the synthesis of various precious-metal NPs. AgNPs, PdNPs, and PtNPs were prepared accordingly with excellent size control. Here, the shape control of nanoparticles remains a challenge. The tailor-made nanocomposites based on cagelike polymer templates are promising for the design of novel functional materials, where both the excellent size control and monofunctionality of Cage-*co*-PMMA are exploited.

Acknowledgements

We are indebted to the Fonds der Chemischen Industrie (Z.F.) and SFB 840 for financial support. We are also indebted to Elitenetzwerk Bayern for assistance with scientific writing.

Keywords: block copolymers · grafting-around · nanoparticles · polymer cages · templates

How to cite: *Angew. Chem. Int. Ed.* **2015**, *54*, 14539–14544
Angew. Chem. **2015**, *127*, 14747–14752

[1] M. Ding, D. C. Sorescu, G. P. Kotchey, A. Star, *J. Am. Chem. Soc.* **2012**, *134*, 3472–3479.
[2] L. Wang, H. Dou, Z. Lou, T. Zhang, *Nanoscale* **2013**, *5*, 2686–2691.
[3] S. Srivastava, J. L. Schaefer, Z. Yang, Z. Tu, L. A. Archer, *Adv. Mater.* **2014**, *26*, 201–234.
[4] A. Rapakousiou, C. Deraedt, H. Gu, L. Salmon, C. Belin, J. Ruiz, D. Astruc, *J. Am. Chem. Soc.* **2014**, *136*, 13995–13998.
[5] O. Shimoni, A. Postma, Y. Yan, A. M. Scott, J. K. Heath, E. C. Nice, A. N. Zelikin, F. Caruso, *ACS Nano* **2012**, *6*, 1463–1472.
[6] F. Mitschang, H. Schmalz, S. Agarwal, A. Greiner, *Angew. Chem. Int. Ed.* **2014**, *53*, 4972–4975; *Angew. Chem.* **2014**, *126*, 5073–5076.
[7] H. Wu, Z. Liu, X. Wang, B. Zhao, J. Zhang, C. Li, *J. Colloid Interface Sci.* **2006**, *302*, 142–148.
[8] S. M. Marinakos, J. P. Novak, L. C. Brousseau III, A. B. House, E. M. Edeki, J. C. Feldhaus, D. L. Feldheim, N. Carolina, *J. Am. Chem. Soc.* **1999**, *121*, 8518–8522.
[9] D. G. Shchukin, I. L. Radtchenko, G. B. Sukhorukov, *J. Phys. Chem. B* **2003**, *107*, 86–90.
[10] T. Valdessolis, P. Vallevigon, M. Sevilla, A. B. Fuertes, *J. Catal.* **2007**, *251*, 239–243.
[11] R. M. Crooks, M. Zhao, L. Sun, V. Chechik, L. K. Yeung, *Acc. Chem. Res.* **2001**, *34*, 181–190.
[12] H. Lang, R. A. May, B. L. Iversen, B. D. Chandler, *J. Am. Chem. Soc.* **2003**, *125*, 14832–14836.
[13] M.-K. Park, S. Deng, R. C. Advincula, *Langmuir* **2005**, *21*, 5272–5277.
[14] X. Tao, J. Li, H. Möhwald, *Chem. Eur. J.* **2004**, *10*, 3397–3403.
[15] A. Samanta, M. Tesch, U. Keller, J. Klingauf, A. Studer, B. J. Ravoo, *J. Am. Chem. Soc.* **2015**, *137*, 1967–1971.
[16] Y. Kang, T. A. Taton, *Angew. Chem. Int. Ed.* **2005**, *44*, 409–412; *Angew. Chem.* **2005**, *117*, 413–416.
[17] K. Ariga, Y. Lvov, T. Kunitake, *J. Am. Chem. Soc.* **1997**, *119*, 2224–2231.
[18] C. Boyer, M. R. Whittaker, C. Nouvel, T. P. Davis, *Macromolecules* **2010**, *43*, 1792–1799.
[19] D. Choi, B. Son, T. H. Park, J. Hong, *Nanoscale* **2015**, *7*, 6703–6711.
[20] H. Long, Y. Jin, A. Sanders, W. Park, W. Zhang, *J. Am. Chem. Soc.* **2014**, *136*, 1782–1785.
[21] J. P. Hermes, F. Sander, U. Fluch, T. Peterle, D. Thompson, R. Urbani, T. Pfohl, M. Mayor, *J. Am. Chem. Soc.* **2012**, *134*, 14674–14677.

[22] C. Krüger, S. Agarwal, A. Greiner, *J. Am. Chem. Soc.* **2008**, *130*, 2710 – 2711.
[23] S. Bokern, K. Gries, H.-H. Görtz, V. Warzelhan, S. Agarwal, A. Greiner, *Adv. Funct. Mater.* **2011**, *21*, 3753 – 3759.
[24] K. Gries, M. El Helou, G. Witte, S. Agarwal, A. Greiner, *Polymer* **2012**, *53*, 1632 – 1639.
[25] Z. Fan, M. Köhn Serrano, A. Schaper, S. Agarwal, A. Greiner, *Adv. Mater.* **2015**, *27*, 3888 – 3893.
[26] D. V. Leff, P. C. Ohara, J. R. Heath, W. M. Gelbart, *J. Phys. Chem.* **1995**, *99*, 7036 – 7041.
[27] J. Chai, X. Liao, L. R. Giam, C. A. Mirkin, *J. Am. Chem. Soc.* **2012**, *134*, 158 – 161.
[28] N. Sakamoto, M. Harada, T. Hashimoto, *Macromolecules* **2006**, *39*, 1116 – 1124.
[29] S. Bokern, K. Volz, S. Agarwal, A. Greiner, *J. Nanopart. Res.* **2012**, *14*, 1041 – 1051.

Received: July 12, 2015
Published online: October 6, 2015

